Excitonic effects in time-dependent density functional theory from zeros of the density response

D. R. Gulevich [1], Ya. V. Zhumagulov [2], V. K. Kozin [3] and I. V. Tokatly [4,5,6,1]

[1]*School of Physics and Engineering, ITMO University, St. Petersburg 197101, Russia*
[2]*Institute for Theoretical Physics, University of Regensburg, Regensburg 93040, Germany*
[3]*Department of Physics, University of Basel, Klingelbergstrasse 82, CH-4056 Basel, Switzerland*
[4]*Nano-Bio Spectroscopy group and European Theoretical Spectroscopy Facility (ETSF), Departamento de Polímeros y Materiales Avanzados: Física, Química y Tecnología, Universidad del País Vasco, Av. Tolosa 72, E-20018 San Sebastián, Spain*
[5]*IKERBASQUE, Basque Foundation for Science, 48009 Bilbao, Spain*
[6]*Donostia International Physics Center (DIPC), 20018 Donostia-San Sebastián, Spain*

We show that the analytic structure of the dynamical exchange-correlation (xc) kernels of semiconductors and insulators can be sensed in terms of its poles, which mark physically relevant frequencies of the system where the counterphase motion of discrete collective excitations occurs: If excited, the collective modes counterbalance each other, making the system exhibit none at all or extremely weak density response. This property can be employed to construct simple and practically relevant approximations of the dynamical xc kernel for time-dependent density functional theory (TDDFT). Such kernels have simple analytic structures, are able to reproduce dominant excitonic features of the absorption spectra of monolayer semiconductors and bulk solids, and promise high potential for future uses in efficient real-time calculations with TDDFT.

I. INTRODUCTION

The time-dependent density functional theory (TDDFT), aiming at extending the density functional theory to the description of electronic excitations and electron dynamics, while being, in principle, exact theory, provides a practically useful alternative to many-body perturbation methods [1]. While the TDDFT owes its popularity in the computational condensed-matter physics and computational chemistry to the adiabatic local density approximation (ALDA), the description of excitonic effects has become a serious challenge, provoking the genuine interest of theorists [2–18]. It has long been understood [2,3] that accounting for the long-range Coulomb-like tail [19] of the exchange-correlation (xc) kernels which is missing in the local xc kernels such as ALDA and generalized gradient approximation is crucial for capturing the excitonic effects. Many subsequent works focused on designing a suitable approximation for xc kernels with suitable long-range behavior [4–13,15,20]. Nevertheless, accounting for the long-range tail via a static approximation [2,6] typically yields a single bound exciton peak while being unable to even qualitatively describe multiple excitonic features exhibited by 2D materials, such as monolayers of transition metal dichalcogenides (TMDCs), whose optical properties are dominated by several well-pronounced bound and continuum excitons [21–24]. Indeed, it is well recognized that nonadiabatic xc effects are responsible for a number of important physical phenomena exhibited by both finite and extended systems, fostering many attempts to understand the nature of nonadiabaticity in TDDFT and to construct consistent frequency-dependent approximations [25–41].

The central object of the linear response TDDFT is the dynamic xc kernel $f_{xc}(\omega, \mathbf{r}, \mathbf{r}')$, which is responsible for all interaction effects beyond the random phase approximation (RPA). The exact xc kernel is formally equal to the difference between inverses of the KS density response function $\chi_s(\omega, \mathbf{r}, \mathbf{r}')$ and the exact irreducible density response function [42] $\tilde{\chi}(\omega, \mathbf{r}, \mathbf{r}')$, that is, $f_{xc}(\omega, \mathbf{r}, \mathbf{r}') = \chi_s^{-1}(\omega, \mathbf{r}, \mathbf{r}') - \tilde{\chi}^{-1}(\omega, \mathbf{r}, \mathbf{r}')$. Remarkably, in the early years of TDDFT, the very existence of the xc kernel for frequencies above the absorption threshold was put in doubt. In 1987, Mearns and Kohn (MK) demonstrated [43] that for finite noninteracting systems the density response function at some special frequencies may have zero eigenvalues, which indicates that there exist time-periodic external potentials causing no density response. Apparently, this implies the noninvertibility of χ_s and, therefore, nonexistence of f_{xc} [44]. Later, it was recognized that the MK zeros do not cause problems for TDDFT. As these zeros are located strictly at the real axis, the response function is always invertible for physical causal dynamics driven by potentials switched on at some initial time [45]. Despite the absence of conceptual difficulties, the existence of MK zeros and the corresponding singularities of f_{xc} are considered as disturbing features of the formalism [1,38,45,46], while their practical importance has remained almost unstudied till now [41].

It is usually assumed that zeros of the density response can appear in some exotic situations and only in the case of finite systems, while they are generically absent in extended systems in the thermodynamic limit (see, e.g., the corresponding discussion in Ref. [1]). In this paper, we show that the MK zeros are in fact very common in the long wavelength density response of solids as they are responsible for nonadiabatic excitonic effects in the optical absorption of semiconductors and insulators. Zeroes of the interacting response function always appear at isolated frequencies between energies of optically
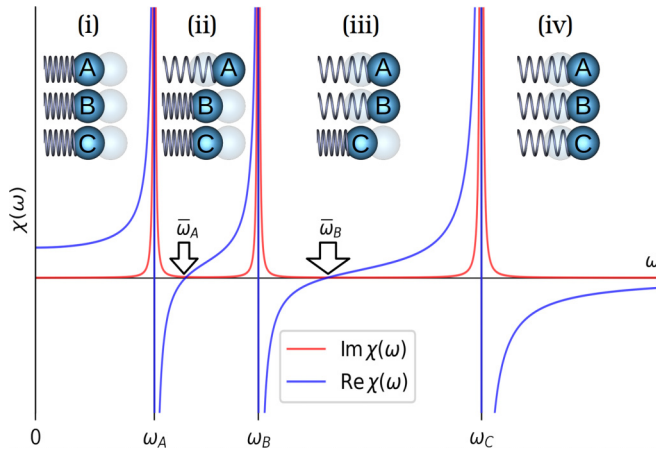
FIG. 1. The real and imaginary parts of the response function $\chi(\omega)$ of a mechanical system possessing eigenmodes A, B, and C illustrated in the plot as independent oscillators. Arrows mark zeros $\bar{\omega}_n$ of the response of a collective variable $P(t)$ which arise as a result of the compensated out-of-phase motion of the oscillators. The insets show their relative phases in different dynamical regimes (i)–(iv).

active excitons. The corresponding poles of f_{xc} represent the key nonadiabatic features required for the TDDFT description of multiple excitonic peaks in the optical spectra. Here we illustrate a general relation between the MK zeros, analytic properties of the xc kernel, and excitonic effects in solids.

The paper is organized as follows. In Sec. II, we demonstrate appearance of zeros of the density response in a simple mechanical toy model. In Sec. III, we highlight the important connection between zeros of the response and the xc kernels in TDDFT, suggesting a path to constructing efficient and practically relevant approximations of f_{xc}. In Sec. IV, we illustrate our approach in practice by applying it to optical absorption in a 2D Dirac model and constructing fully analytic f_{xc} capable of recovering the full Rydberg series of excitonic peaks within the TDDFT. In Secs. V and VI, we demonstrate the application of our approach to designing minimalistic frequency-dependent xc kernels sufficient for reproducing the dominant features of optical spectra of the paradigmatic monolayer TMDCs and bulk solids. In Sec. VII, we discuss the possible impact of our paper and its future prospects for highly efficient real-time calculations using TDDFT.

II. ZEROS OF THE RESPONSE FUNCTION

Let us first illustrate the significance and the formal origin of zeros in the response function in a simple toy model. Consider a mechanical system with three nondegenerate eigenmodes $\omega_A < \omega_B < \omega_C$ illustrated by independent mechanical oscillators A, B, and C in Fig. 1 and coupled to a periodic external field $E(t) = E(\omega)e^{-i\omega t}$ in and in the presence of a small damping $\eta \ll \omega_n$:

$$\ddot{x}_n = -\omega_n^2 x_n - 2\eta \dot{x}_n + Z_n E(t), \quad n = A, B, \text{ and } C. \quad (1)$$

Here, Z_n play the role of charges of the oscillators. In an ideal isolated system, the damping η can be understood as the adiabatic parameter describing the periodic drive slowly switched on at $t \to -\infty$. Suppose the object of interest is the

collective variable, conjugated to the driving field $E(t)$:

$$P(t) = \sum_n Z_n x_n(t). \quad (2)$$

Thus, the quantity $P(t)$ yields the net polarization induced by the external field. For the linear response function $\chi(\omega)$ defined by $P(\omega) = \chi(\omega)E(\omega)$, we obtain

$$\chi(\omega) = -\sum_n \frac{Z_n^2}{\omega^2 - \omega_n^2 + 2i\omega\eta}. \quad (3)$$

The singularities of the response function $\chi(\omega)$ at ω_n divide the positive real axis (similarly, for the negative frequency axis) into several domains which correspond to qualitatively different dynamical regimes: (i) $\omega < \omega_A$: all modes oscillate in phase with the external drive, (ii) $\omega_A < \omega < \omega_B$: mode A is out of phase, while B and C are in phase with the external drive, (iii) $\omega_B < \omega < \omega_C$: A and B are out of phase and C is in phase with the external drive, and (iv) $\omega_C < \omega$: all modes are out of phase with the external drive, see Fig. 1. In the intermediate regimes (ii) and (iii), there are two special points denoted by $\bar{\omega}_A$ and $\bar{\omega}_B$ in Fig. 1 where the contributions of modes A, B, and C to the response counterbalance each other—these are zeros of $\chi(\omega)$ (which coincide with zeros of the $\mathrm{Re}\,\chi(\omega)$ in the case of the vanishing imaginary part), where the net polarization is practically absent. Importantly, for real frequencies ω and finite η, the response is never *exactly* zero while the inverse $\chi^{-1}(\omega)$ is well-defined everywhere, which is, of course, a manifestation of the general statement by van Leeuwen [45]. However, by slowing down the switching process or by waiting sufficiently long after a sudden switch on, one can make the response at the above two special frequencies arbitrary weak. These two special points are the MK zeros for our toy model.

The formal reason for existence of a zero response is that the number of microscopic degrees of freedom, defining the number of physical resonances, is larger than the dimension of space hosting the collective variable—in our toy model example, 3 and 1, respectively. It is worth noting that a similar counting argument was used to prove the possibility of zero eigenvalues for the one-particle Green's function in interacting systems [47]. In the specific case of the density response, one can rephrase this differently: the set of transition densities is always overcomplete in the functional space hosting the density variations. Loosely speaking, there are more excitations (resonances) than eigenfunctions spanning the space of densities. As a result, several resonances may, in general, contribute to one eigenvalue, and the out-of-phase dynamics of densities for different resonances will produce zero response at isolated frequencies in exactly the same way as shown in Fig. 1.

It is worth emphasizing that the presence of resonances in the dynamic response/correlation function does not automatically imply the existence of zero eigenvalues between resonant frequencies. The simplest examples are the density response function in a one-particle system (e.g., the hydrogen atom) and the one-particle Green's function in noninteracting many-particle system. In both cases, in spite of the resonant structure, there are no zero eigenvalues because the dimension of the excitation's space that determines the number of

resonances coincides with the dimension of the Hilbert space where the correlation function acts as a linear operator. As a result, there is strictly one resonance per eigenvalue and thus no zeros. Only by adding more particles in the case of the density response or switching on the interaction in the case of the Green's function can we make the number of excitations larger than the number of the eigenvalues of the correlation function, which opens a possibility for the appearance of zeros. Our toy model is aimed at demonstrating exactly this point, which is apparently very general for any dynamical theory of reduced/collective variables, such as TDDFT.

Despite its apparent simplicity, the response of this mechanical toy model and the very appearance of this kind of invisibility point at frequencies where no net response is observed, shed light on the analytic structure of the dynamical xc kernel which we will discuss in the next section.

III. ANALYTIC STRUCTURE OF THE DYNAMICAL LONG-RANGE XC KERNEL

Having discussed the origin of zeros in the response in a simple mechanical model, we now focus our attention on many-electron systems. Throughout the paper, we will be using Hartree atomic units ($\hbar = m_0 = e = 1$), unless specified otherwise, where expressing the frequencies in units of eV is more natural.

Consider a material with the energy gap, such as semiconductor or insulator. In general, in solids the response function $\chi_{\mathbf{G},\mathbf{G}'}(\omega, q)$ becomes a matrix in the reciprocal lattice vectors $\mathbf{G}$. The same is obviously true for the xc kernel. However, the excitonic absorption is typically dominated by the head of this matrix (the element with $\mathbf{G} = \mathbf{G}' = 0$). Indeed, the head of the density response functions of a gapped material at small momentum $q \to 0$ behaves as $\sim q^2$ [48,49], which implies the famous $1/q^2$ singularity in the head of the xc kernel. Thus, by restricting our attention to the heads of the above matrices, we can separate the spatial and frequency-dependent parts by introducing $\chi(q, \omega) = q^2 \beta(\omega)$, $\chi_s(q, \omega) = q^2 \beta_s(\omega)$, and $f_{xc}(q, \omega) = \alpha(\omega)/q^2$ related by

$$\alpha(\omega) = \frac{1}{\beta_s(\omega)} - \frac{1}{\beta(\omega)}. \tag{4}$$

This allows us to focus our attention on the frequency-dependent parts exclusively. In the RPA, the response function has no singularities below the onset of the e-h continuum. Accounting for the exchange and correlation effects results in redistribution of the oscillator strengths and appearance of discrete exciton states with energies ω_n and oscillator strengths $X_n > 0$ inside the fundamental gap Δ,

$$\beta(\omega) = \sum_n \frac{X_n}{\omega^2 - \omega_n^2} + \beta^{\text{reg}}(\omega), \tag{5}$$

where the first and second contributions arise from the discrete ($\omega_n < \Delta$) and continuum spectrum, respectively. We introduced the subscript reg to highlight that the continuum spectrum contribution $\beta^{\text{reg}}(\omega)$ is a regular function with no singularities inside the fundamental gap. Because $|\beta^{\text{reg}}(\omega)| < \infty$ for $\omega < \Delta$ and the oscillator strengths, being proportional to the square of the associate transition dipole elements are positive ($X_n > 0$), the series of singularities $\{\omega_n\}$ is

alternating with the series of zeros $\{\bar{\omega}_n\}$, in direct analogy with the mechanical toy model (cf. Fig. 1).

It has been shown by one of us in Ref. [20] that the quasiparticle and excitonic parts of the xc kernel can be treated separately. Thus, we assume that the scissor correction has been applied to $\beta_s(\omega)$, so $\beta_s(\omega)$ and $\beta(\omega)$ have the same gap energy Δ, while focusing on the excitonic contribution only. Because $\beta(\omega)$ enters Eq. (4) as the inverse, there arises a correspondence of zeros in the response to singularities of $\alpha(\omega)$. Let us separate these from the xc kernel explicitly. For the imaginary part of $\alpha(\omega)$, we have

$$\text{Im}\, \alpha(\omega) = \Theta(\omega^2 - \Delta^2)\, \text{Im}\left[\frac{1}{\beta_s(\omega)} - \frac{1}{\beta(\omega)}\right]$$
$$+ \sum_n \frac{\pi}{\beta'(\bar{\omega}_n)}[\delta(\omega - \bar{\omega}_n) - \delta(\omega + \bar{\omega}_n)], \tag{6}$$

where by $\bar{\omega}_n$ we label the smallest zero higher than ω_n, so $\omega_n < \bar{\omega}_n < \omega_{n+1}$. The full complex function $\alpha(\omega)$ is given by the sum of a regular part which has no singularities inside the fundamental gap and a number of discrete poles,

$$\alpha(\omega) = \alpha^{\text{reg}}(\omega) + \sum_n \frac{F_n}{\omega^2 - \bar{\omega}_n^2}, \tag{7}$$

with positive oscillator strengths:

$$F_n = -\frac{2\bar{\omega}_n}{\beta'(\bar{\omega}_n)} > 0. \tag{8}$$

The real and imaginary parts of $\alpha^{\text{reg}}(\omega)$ are related by the Kramers-Kronig transform and are then defined by

$$\text{Im}\, \alpha^{\text{reg}}(\omega) = \Theta(\omega^2 - \Delta^2)\, \text{Im}\left[\frac{1}{\beta_s(\omega)} - \frac{1}{\beta(\omega)}\right],$$
$$\text{Re}\, \alpha^{\text{reg}}(\omega) = \alpha(\infty) + \frac{1}{\pi}\mathcal{P}\int_{-\infty}^{\infty} \frac{\omega'\, \text{Im}\, \alpha^{\text{reg}}(\omega)}{\omega'^2 - \omega^2} d\omega'. \tag{9}$$

As seen from Eqs. (7) and (8), zeros of the response define the poles of the xc kernel with the strengths given by the slope of the response function at its zeros.

To summarize, Eqs. (6) and (7) illustrate that the dynamical part of the xc kernel $\alpha(\omega)$ has poles at special frequencies $\{\bar{\omega}_n\}$ where no response to external perturbation is observed, owing to the counterbalanced contributions of the discrete modes. Each of these special frequencies is located strictly between the subsequent pairs of physical excitations. In the following section, we will demonstrate the dynamical xc kernel and the associated pole structure given by Eq. (7) in application to the 2D massive Dirac (2DMD) model.

IV. 2D MASSIVE DIRAC MODEL

Capturing the excitonic effects is one of the long-standing difficulties of TDDFT. While the ALDA fails to reproduce excitonic peaks at all, the static long-range corrected (LRC) kernel [2,6,7,9,13,15,19] with the $\alpha(\omega)$ approximated by a constant $\alpha(\omega) = -\alpha_{\text{static}}$, is only capable of capturing single excitonic peak. Although the attempt to go beyond the static approximation by including a quadratic frequency-dependence in Ref. [36] demonstrated some improvement in the numerically calculated dielectric function of semiconductors, it is still too simplistic to be applied to 2D

semiconductors where excitonic phenomena are dominant features of the absorption spectrum possessing multiple excitonic peaks. In this section, we employ the 2DMD model to illustrate a simple approximation to the dynamical xc kernel arising from the representation Eq. (7), which is capable of capturing not only an isolated exciton peak but the full Rydberg series of excitonic excitations. We consider spinless single valley 2DMD model with Hamiltonian

$$H_0 = v(k_x \sigma_x + k_y \sigma_y) + \frac{\Delta}{2} \sigma_z, \quad (10)$$

with interaction between Dirac fermions described by the Rytova-Keldysh potential [50–52]:

$$W_{RK}(q) = -\frac{2\pi}{\varepsilon \, q(1 + r_0 q)}. \quad (11)$$

Here, ε is the dielectric constant and r_0 is the screening length [53,54]. The single-particle 2DMD Eq. (10) has been shown to appear as a $k.p$ model in TMDC monolayers as a result of interplay between the inversion symmetry breaking and spin-orbit coupling [55]. Taking Coloumb interaction into consideration results in the appearance of Rytova-Keldysh potential Eq. (11) arising as a result of 2D screening [50–52].

The analytical expression for $\beta_s(\omega)$ follows from the polarization bubble diagram (see, e.g., Ref. [56]):

$$\beta_s(\omega) = \frac{v^2}{8\pi\omega} \left[\frac{\Delta}{\omega} - \left(1 + \frac{\Delta^2}{\omega^2}\right) \text{arctanh} \frac{\omega}{\Delta} \right]. \quad (12)$$

The absorption spectra for the 2DMD model in the subgap region are dominated by the s states. Explicit formulas for exciton binding energies of s states in 2D TMDC monolayers were given in the literature [57–59]. Employing the effective mass approximation, we use the following semiempirical formula for s states (Eq. (3) of Ref. [59]) upon the replacement of μ by $5\mu/4$ [60]):

$$E_n = -\frac{5}{2\mu r_0^2} \left[\sqrt{n - \frac{1}{2} + \sqrt{\frac{2\mu r_0}{\varepsilon}}} - \sqrt{n - \frac{1}{2}} \right]^4. \quad (13)$$

Because the location of zeros of $\chi(\omega)$ is restricted from both sides by adjacent s excitons, a reasonable estimate for $\bar{\omega}_n$ is provided by extending Eq. (13) to fractional arguments and evaluating it at an intermediate value $n + \nu$ between n and $n + 1$ with $0 < \nu < 1$. Thus, we take

$$\bar{\omega}_n = \Delta + E_{n+\nu} \quad (14)$$

and evaluate it at a central value $\nu = 0.5$ [61]. Our numerical results suggest that the oscillator strengths F_n follow an empirical trend

$$F_n \approx 8\varepsilon v \bar{\omega}_n \Delta \left(1 - \frac{\bar{\omega}_n}{\Delta}\right)^{3/2}, \quad (15)$$

which is nearly independent of r_0. Approximating the regular part $\alpha^{reg}(\omega)$ by a constant

$$\alpha^{reg}(\omega) \approx \alpha(\infty) = \text{const}, \quad (16)$$

and using Eqs. (14)–(16), one obtains the simplest parametrization of $\alpha(\omega)$ for the 2DMD model capable of capturing the full exciton Rydberg series.
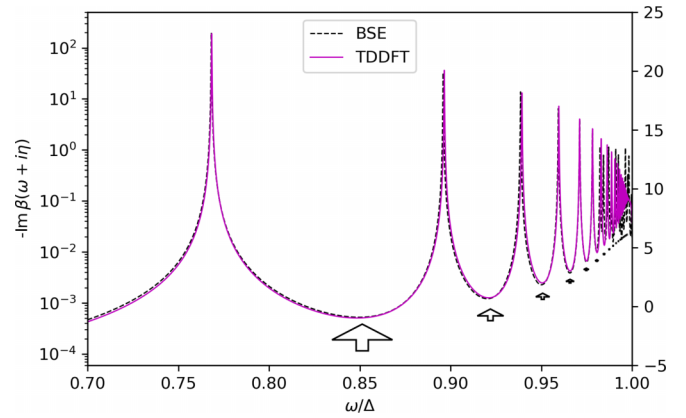
FIG. 2. Imaginary part of the response function $\beta(\omega + i\eta)$ for the massive Dirac model obtained using our parametrization of the dynamical xc kernel (TDDFT, solid line). For comparison, the result of solution of the Bethe-Salpeter equation in Tamm-Dancoff approximation is shown (BSE, dashed line). An artificial broadening $\eta/\Delta = 10^{-4}$ was used to smear the singularities. Arrows indicate poles of the xc kernel located at zeros of the response $\bar{\omega}_n$ in accordance with Eq. (7). The arrow sizes are scaled with the pole strengths F_n. The BSE spectrum is unconverged in the vicinity of the gap due to the finite mesh size and manifests itself as unphysical erratic oscillations at $\omega/\Delta \gtrsim 0.98$.

To verify this parametrization, we compare the TDDFT response function to the response function obtained by solving the Bethe-Salpeter equation (BSE) [62]. In the calculations, we employed the Tamm-Dancoff approximation which neglects antiresonant terms of the spectra (see, e.g., similar studies in Refs. [63,64]). For illustration, we take $\varepsilon = 1$, $\Delta = 2.5$ eV, $r_0 = 35$ Å, and $\mu = 0.20 \, m_0$, which, apart from the spin and valley degrees of freedoms ignored here, are typical for the TMDC monolayers (see, e.g., the Supplemental Material of Ref. [59]). The results for $\text{Im} \chi(\omega + i\eta)$ with broadening $\eta/\Delta = 10^{-4}$ are shown in Fig. 2. The remaining parameter $\alpha(\infty) = -9.7$ was chosen to match the lowest exciton peak to that of the BSE calculation.

V. 2D MATERIALS

In the case of *ab initio* calculations of optical properties of real materials, the high resolution we used to reproduce the Rydberg series in the previous section is redundant. In fact, the experimental absorption spectra of 2D monolayers exhibit few dominant features—*A* and *B* exciton peaks related to the spin-orbit splitting of the Dirac-like dispersion at the *K* point of the Brillouin zone and a prominent *C* peak above the quasiparticle gap are attributed to excitonic transitions from multiple points around the Γ point [22,65]. Accounting for only these three dominant features returns us to the analogy with the mechanical model of three oscillators discussed in Sec. II. In direct analogy with Fig. 1, there arise two zeros of the response $\bar{\omega}_A$ and $\bar{\omega}_B$ which result from the mutual compensation of *A*, *B*, and *C* excitations and which are of practical importance for reconstructing the xc kernel. Approximating the regular part by a constant $\alpha^{reg}(\omega) \approx \alpha(\infty)$, Eq. (7) reads

$$\alpha(\omega) = \alpha(\infty) + \sum_n \frac{F_n}{\omega^2 - \bar{\omega}_n^2}. \quad (17)$$

TABLE I. Parametrization of the dynamical xc kernel for 2D monolayers and bulk materials. Values of $\alpha(\infty)$ are given in Hartree atomic units. For convenience, $\bar{\omega}_n$ and F_n are expressed in eV and eV^2, respectively, to restore the result for $\alpha(\omega)$ in atomic units.

Material	$\alpha(\infty)$	$\bar{\omega}_1$	F_1	$\bar{\omega}_2$	F_2	$\bar{\omega}_3$	F_3	$\bar{\omega}_4$	F_4	$\bar{\omega}_5$	F_5
1L WS$_2$ on SiO$_2$	-1.2	2.074	0.125	2.466	0.185						
1L MoS$_2$ on SiO$_2$	-0.9	1.876	0.030	2.037	0.060						
LiF	-7.0	13.6	40.0								
Solid Ar	-6.7	12.15	1.6	12.70	57.0	13.60	4.0	13.79	2.0	13.94	1.0

It is common to characterize the excitonic contributions to dielectric function of 2D materials obtained in experiments in terms of Lorentz and Tauc-Lorentz oscillators [24,66–69]. It is therefore practically useful to parametrize the $\alpha(\omega)$ in terms of these quantities. Recently [68,69], the Tauc-Lorentz parameters for *A, B,* and *C* peaks of MoS$_2$ monolayer were provided. Assuming the frequencies ω_n and oscillator strengths X_n of *A*, *B*, and *C* peaks are given, we can find the poles and their strengths of $\alpha(\omega)$ directly. Because the *C* peak dominates over *A* and *B*, the counterbalance points [aka zeros of $\chi(\omega)$] occur right in the vicinity of the *A* and *B* resonances. In this case, zeros can be easily found perturbatively. Denoting by $\beta_n^{\mathrm{reg}}(\omega)$ the regular part of $\beta(\omega)$ with the contribution of the *n*th pole subtracted, the zero $\bar{\omega}_n$ is defined by

$$\frac{X_n}{\bar{\omega}_n^2 - \omega_n^2} + \beta_n^{\mathrm{reg}}(\bar{\omega}_n) = 0. \tag{18}$$

Taking $\beta_n^{\mathrm{reg}}(\bar{\omega}_n) \approx \beta_n^{\mathrm{reg}}(\omega_n)$ as the zeroth order, $\bar{\omega}_n$ can then be found iteratively. To find the oscillator strengths, we neglect the slowly varying regular part $\beta_n^{\mathrm{reg}}(\omega)$ and obtain

$$F_n = -\frac{2\bar{\omega}_n}{\beta'(\bar{\omega}_n)} \approx \frac{\left(\bar{\omega}_n^2 - \omega_n^2\right)^2}{X_n} = \frac{X_n}{\beta_n^{\mathrm{reg}}(\bar{\omega}_n)^2}. \tag{19}$$

We use the experimental data from Ref. [68] for WS$_2$ monolayer on SiO$_2$ substrate and [69] for MoS$_2$ monolayer on SiO$_2$ substrate with perylene-3,4,9,10-tetracarboxylic acid tetrapotassium salt molecule, parametrized in the form of Tauc-Lorentz oscillators. From the parameters of oscillators we extract the positions and oscillator strength of the Lorentzian exciton peaks and apply Eqs. (18) and (19) to find the poles and strengths of the dynamical xc kernel summarized in the Table I.

To test the obtained parametrization, we used the *ab initio* code `exciting` [70]. The band structures of the monolayers were calculated using the LDA functional, accounting for the spin-orbit coupling. For the linear response calculations, we applied the scissor correction 0.54 and 0.82 eV for MoS$_2$ and WS$_2$, respectively, to adjust the fundamental band gap to the experimentally measured values 2.16 eV for MoS$_2$ and 2.38 eV for WS$_2$ monolayers on quartz substrate [71]. As we are interested in the in-plane component of the response, local field effects were ignored in this paper due to their minor effect on the in-plane polarization. The results of our calculation using TDDFT employing the parametrization from Table I are shown in Fig. 3. In the RPA calculations, we used artificial broadening $\eta_{\mathrm{RPA}} = 0.1$ eV. In the context of TDDFT, while η_{RPA} is responsible for broadening the subgap absorption in the continuum, the widths of bound excitons can be tuned by

shifting the argument of xc kernel $\alpha(\omega) \to \alpha(\omega + i\eta_{\mathrm{xc}})$. We used $\eta_{\mathrm{xc}} = 0.03$ for WS$_2$ and $\eta_{\mathrm{xc}} = 0.015$ eV for MoS$_2$. Finally, the value of the only remaining parameter $\alpha(\infty)$ weakly affects positions of exciton peaks and was chosen so to match the resulting peak strengths to the experimentally observed values.
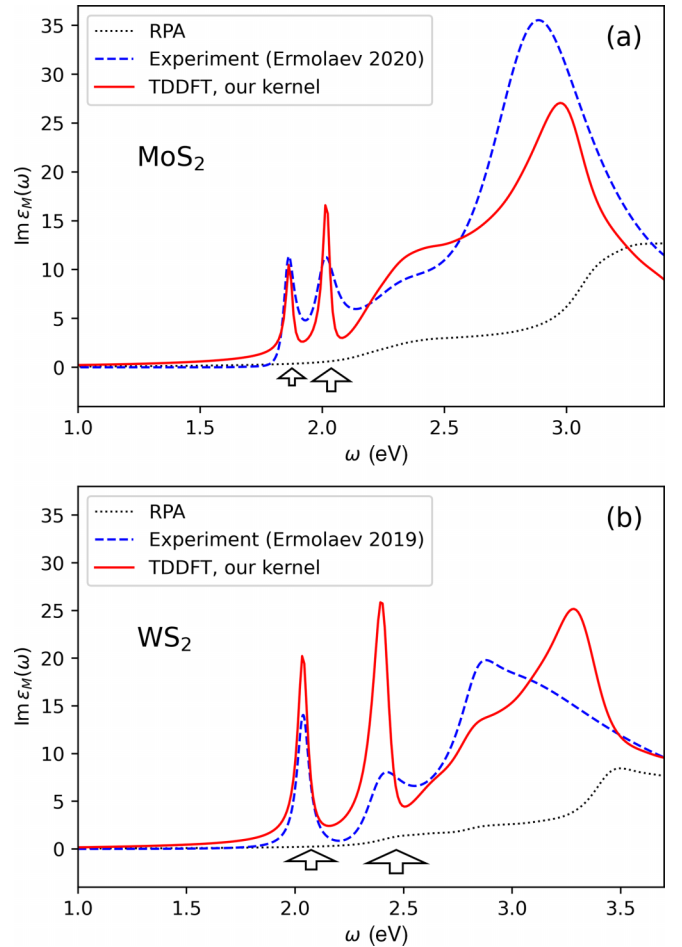
FIG. 3. Dielectric function of MoS$_2$ (a) and WS$_2$ (b) monolayers calculated using the linear-response TDDFT (black solid curve) with the *ab initio* `exciting` code [70] and the parametrization of the dynamic xc kernel given by the Eq. (17) with parameters specified in Table I. The dashed blue curve marks the experimental data for MoS$_2$ and WS$_2$ monolayers on SiO2 substrate from Refs. [69] and [68]), respectively, used to derive the parameters of parametrization. The dotted curve shows the RPA result. Arrows indicate poles of the xc kernel located at zeros of the response $\bar{\omega}_n$. The arrow sizes are scaled with the pole strengths F_n.
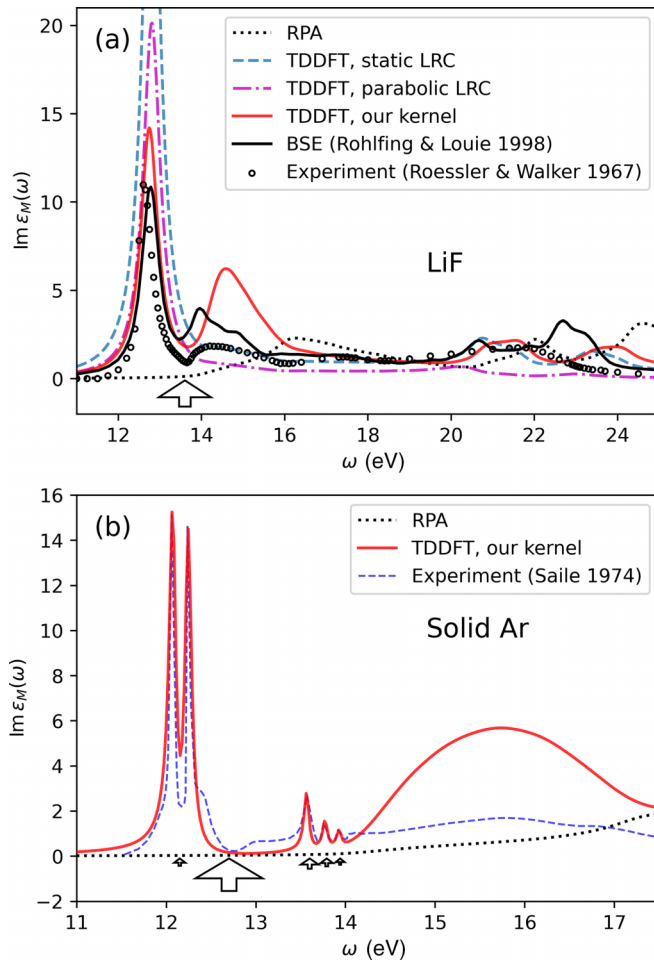
FIG. 4. Imaginary part of the dielectric function for LiF (a) and solid Ar (b). Aritificial homogeneous broadening has been used $\eta_{xc} = \eta_{RPA} = 0.25$ eV [same for $\alpha(\omega)$ and RPA] for LiF to match the broadening in the BSE result [72]. The broadenings for solid Ar are $\eta_{xc} = 0.03$ eV and $\eta_{RPA} = 0.25$ eV. The experimental data is taken from Refs. [84,85] for LiF and Ar, respectively. Arrows indicate locations of the poles of the xc kernel at zeros of the response $\bar{\omega}_n$. The arrow sizes are scaled with the pole strengths F_n.

VI. BULK SOLIDS

Similar to the case of 2D materials discussed above, the same approach applies to bulk wide-gap semiconductors and insulators exhibiting bound excitons in the absorption spectra. Some of the illustrative examples are LiF and solid Ar, which have received a great deal of attention in a range of theoretical studies [4,15,72–76].

The experimental absorption spectrum of LiF exhibits a pronounced excitonic peak at 12.6 eV followed by an unresolved Rydberg series [77] and a featureless quasiparticle band gap at 14.1–14.2 eV [78], see Fig. 4(a). We therefore should expect the zero of the response function to appear between the first exciton and the onset of the Rydberg series at 13.6 eV. By placing a pole at $\bar{\omega}_1 = 13.6$ eV, we obtain a simple one-pole parametrization of the xc kernel for LiF presented in Table I. The results obtained using the static [2,6] and parabolic [36] LRC kernels are also shown in Fig. 4(a) for

comparison [79]. The presence of the pole redistributes the oscillator strengths toward higher energies, causing a secondary peak at 14.5 eV, which is present in BSE and experiments but absent in the static and parabolic LRC approaches. Moreover, in contrast to the parabolic LRC, our xc kernel does not suppress the absorption at higher energies, as seen in Fig. 4(a). For ease of comparison with BSE calculations, we used the same broadening $\eta_{xc} = \eta_{RPA} = 0.25$ eV as used in Ref. [72].

The absorption spectrum of solid Ar consists of a series of well-separated exciton peaks [80–82]. In the same fashion, accounting for the dominant $n = 1$, $1'$, 2, $2'$ and 3 excitonic features, we obtain the parametrization for the xc kernel presented in Table I. The dielectric function calculated results using this parametrization are presented in Fig. 4(b). We used artificial broadenings $\eta_{RPA} = 0.25$ eV and $\eta_{xc} = 0.03$ eV in RPA and $\alpha(\omega)$, respectively. It is interesting to note that the two lowest exciton states $n = 1$, $1'$ are well separated from the rest of the spectra. In this case of two isolated excitonic peaks, the analytic structure of $f_{xc}(\omega)$ has a remarkable analogy to that for double excitations in finite systems, where a pole in the frequency dependence of the xc kernel is shown to appear [32,41,83]. In both systems, the pole in $f_{xc}(\omega)$ reflects the presence of two nonorthogonal excitation channels, which interfere destructively, leading to the suppression of the response at some isolated frequency.

VII. DISCUSSION

We demonstrate that zero eigenvalues of the density response function, discovered many years ago by MK for model systems, represent a common feature of the optical absorption in insulating solids. In fact, they dominate the frequency dependence of the xc kernel of TDDFT, especially when several excitonic peaks, both bound and continuum, are present in the absorption spectra. The latter is especially relevant for insulating materials of reduced dimension, such as TMDC. Shedding light on the nature of nonadiabatic effects in the TDDFT of excitonic absorption, which are characterized by the poles of the dynamical xc kernels, allows us to design simple and practically efficient approximations of the kernels for the *ab initio* description of the collective many-body phenomena within TDDFT. Our approach, illustrated for TMDC monolayers and bulk materials, hints at the procedure for obtaining simple and practical dynamical xc kernels for a variety of semiconducting and insulating materials directly from experimental absorption spectra. The algorithm for reconstructing xc kernels can appear as follows: (i) The experimentally obtained imaginary part of the macroscopic dielectric function is parametrized in terms of Lorentz oscillators. (ii) With the peak widths of the oscillators discarded, the central frequencies and oscillator strengths are used to find poles and oscillator strengths of the xc kernel with the help of Eqs. (18) and (19). (iii) The regular part of the dynamical xc kernel is approximated by a constant $\alpha^{reg}(\omega) \approx \alpha(\infty)$.

Apart from the physical insight, xc kernels in the form Eq. (17) provide a natural tool for the highly efficient practical implementation of the real-time TDDFT. Indeed, while the approach [86] summarizes the scheme for the

calculation using the static LRC kernel, the pole expansion used in Eq. (17) enables us to extend this further to deal with the frequency-dependent kernels with the help of the highly efficient numerical approach proposed in Ref. [87], where the performance comparable to that of the standard time-dependent ALDA has been demonstrated for the case of the Vignale-Kohn functional [26,28]. Based on this, the perspectives of the real-time *ab initio* dynamics with the help of TDDFT and accounting for excitonic effects thus emerge at full scale, which in the case of TMDC monolayer alone is of high practical and fundamental interest. The real-time calculations with TDDFT with the proper accounting of excitonic phenomena may shed light on the intriguing nonlinear phenomena [88,89] while paving the way to a practical impact on semiconducting physics, materials science, and optoelectronics.

[1] C. A. Ullrich, *Time-Dependent Density-Functional Theory: Concepts and Applications* (Oxford University Press, New York, 2012).

[2] L. Reining, V. Olevano, A. Rubio, and G. Onida, Excitonic Effects in Solids Described by Time-Dependent Density-Functional Theory, Phys. Rev. Lett. **88**, 066404 (2002).

[3] Y.-H. Kim and A. Görling, Excitonic Optical Spectrum of Semiconductors Obtained by Time-Dependent Density-Functional Theory with the Exact-Exchange Kernel, Phys. Rev. Lett. **89**, 096402 (2002).

[4] A. Marini, R. Del Sole, and A. Rubio, Bound Excitons in Time-Dependent Density-Functional Theory: Optical and Energy-Loss Spectra, Phys. Rev. Lett. **91**, 256402 (2003).

[5] F. Sottile, V. Olevano, and L. Reining, Parameter-Free Calculation of Response Functions in Time-Dependent Density-Functional Theory, Phys. Rev. Lett. **91**, 056402 (2003).

[6] S. Botti, F. Sottile, N. Vast, V. Olevano, L. Reining, H.-C. Weissker, A. Rubio, G. Onida, R. Del Sole, and R. W. Godby, Long-range contribution to the exchange-correlation kernel of time-dependent density functional theory, Phys. Rev. B **69**, 155112 (2004).

[7] S. Botti, A. Schindlmayr, R. D. Sole, and L. Reining, Time-dependent density-functional theory for extended systems, Rep. Prog. Phys. **70**, 357 (2007).

[8] V. Turkowski, A. Leonardo, and C. A. Ullrich, Time-dependent density-functional approach for exciton binding energies, Phys. Rev. B **79**, 233201 (2009).

[9] S. Sharma, J. K. Dewhurst, A. Sanna, and E. K. U. Gross, Bootstrap Approximation for the Exchange-Correlation Kernel of Time-Dependent Density-Functional Theory, Phys. Rev. Lett. **107**, 186401 (2011).

[10] V. U. Nazarov and G. Vignale, Optics of Semiconductors from Meta-Generalized-Gradient-Approximation-Based Time-Dependent Density-Functional Theory, Phys. Rev. Lett. **107**, 216402 (2011).

[11] Z.-h. Yang and C. A. Ullrich, Direct calculation of exciton binding energies with time-dependent density-functional theory, Phys. Rev. B **87**, 195204 (2013).

[12] C. A. Ullrich and Z.-h. Yang, Excitons in time-dependent density-functional theory, *Density-Functional Methods for*

Excited States, edited by N. Ferré, M. Filatov, and M. Huix-Rotllant (Springer, Cham, 2014), Vol. 368.

[13] S. Rigamonti, S. Botti, V. Veniard, C. Draxl, L. Reining, and F. Sottile, Estimating Excitonic Effects in the Absorption Spectra of Solids: Problems and Insight from a Guided Iteration Scheme, Phys. Rev. Lett. **114**, 146402 (2015).

[14] J. A. Berger, Fully Parameter-Free Calculation of Optical Spectra for Insulators, Semiconductors, and Metals from a Simple Polarization Functional, Phys. Rev. Lett. **115**, 137402 (2015).

[15] Y.-M. Byun and C. A. Ullrich, Assessment of long-range-corrected exchange-correlation kernels for solids: Accurate exciton binding energies via an empirically scaled bootstrap kernel, Phys. Rev. B **95**, 205136 (2017).

[16] S. Cavo, J. A. Berger, and P. Romaniello, Accurate optical spectra of solids from pure time-dependent density functional theory, Phys. Rev. B **101**, 115109 (2020).

[17] S. Di Sabatino, J. A. Berger, and P. Romaniello, Optical spectra of 2D monolayers from time-dependent density functional theory, Faraday Discuss. **224**, 467 (2020).

[18] Y. Suzuki and K. Watanabe, Excitons in two-dimensional atomic layer materials from time-dependent density functional theory: Mono-layer and bi-layer hexagonal boron nitride and transition-metal dichalcogenides, Phys. Chem. Chem. Phys. **22**, 2908 (2020).

[19] P. Ghosez, X. Gonze, and R. W. Godby, Long-wavelength behavior of the exchange-correlation kernel in the Kohn-Sham theory of periodic systems, Phys. Rev. B **56**, 12811 (1997).

[20] R. Stubner, I. V. Tokatly, and O. Pankratov, Excitonic effects in time-dependent density-functional theory: An analytically solvable model, Phys. Rev. B **70**, 245119 (2004).

[21] K. F. Mak, C. Lee, J. Hone, J. Shan, and T. F. Heinz, Atomically Thin MoS_2: A New Direct-Gap Semiconductor, Phys. Rev. Lett. **105**, 136805 (2010).

[22] D. Y. Qiu, F. H. da Jornada, and S. G. Louie, Optical Spectrum of MoS_2: Many-Body Effects and Diversity of Exciton States, Phys. Rev. Lett. **111**, 216805 (2013).

[23] Z. Ye, T. Cao, K. O'brien, H. Zhu, X. Yin, Y. Wang, S. G. Louie, and X. Zhang, Probing excitonic dark states in single-layer tungsten disulphide, Nature (London) **513**, 214 (2014).

[24] A. Chernikov, T. C. Berkelbach, H. M. Hill, A. Rigosi, Y. Li, B. Aslan, D. R. Reichman, M. S. Hybertsen, and T. F. Heinz, Exciton Binding Energy and Nonhydrogenic Rydberg Series in Monolayer WS_2, Phys. Rev. Lett. **113**, 076802 (2014).

[25] E. K. U. Gross and W. Kohn, Local Density-Functional Theory of Frequency-Dependent Linear Response, Phys. Rev. Lett. **55**, 2850 (1985); **57**, 923(E) (1986).

[26] G. Vignale and W. Kohn, Current-Dependent Exchange-Correlation Potential for Dynamical Linear Response Theory, Phys. Rev. Lett. **77**, 2037 (1996).

[27] J. F. Dobson, M. J. Bünner, and E. K. U. Gross, Time-Dependent Density Functional Theory Beyond Linear Response: An Exchange-Correlation Potential with Memory, Phys. Rev. Lett. **79**, 1905 (1997).

[28] G. Vignale, C. A. Ullrich, and S. Conti, Time-Dependent Density Functional Theory Beyond the Adiabatic Local Density Approximation, Phys. Rev. Lett. **79**, 4878 (1997).

[29] I. V. Tokatly and O. Pankratov, Many-Body Diagrammatic Expansion in a Kohn-Sham Basis: Implications for Time-Dependent Density Functional Theory of Excited States, Phys. Rev. Lett. **86**, 2078 (2001).

[30] I. V. Tokatly, R. Stubner, and O. Pankratov, Many-body diagrammatic expansion for the exchange-correlation kernel in time-dependent density functional theory, Phys. Rev. B **65**, 113107 (2002).

[31] R. Del Sole, G. Adragna, V. Olevano, and L. Reining, Long-range behavior and frequency dependence of exchange-correlation kernels in solids, Phys. Rev. B **67**, 045207 (2003).

[32] N. T. Maitra, F. Zhang, R. J. Cave, and K. Burke, Double excitations within time-dependent density functional theory linear response, J. Chem. Phys. **120**, 5932 (2004).

[33] U. von Barth, N. E. Dahlen, R. van Leeuwen, and G. Stefanucci, Conserving approximations in time-dependent density functional theory, Phys. Rev. B **72**, 235109 (2005).

[34] J. I. Fuks, L. Lacombe, S. E. B. Nielsen, and N. T. Maitra, Exploring non-adiabatic approximations to the exchange-correlation functional of TDDFT, Phys. Chem. Chem. Phys. **20**, 26145 (2018).

[35] P. Romaniello, D. Sangalli, J. A. Berger, F. Sottile, L. G. Molinari, L. Reining, and G. Onida, Double excitations in finite systems, J. Chem. Phys. **130**, 044108 (2009).

[36] S. Botti, A. Fourreau, F. Nguyen, Y.-O. Renault, F. Sottile, and L. Reining, Energy dependence of the exchange-correlation kernel of time-dependent density functional theory: A simple model for solids, Phys. Rev. B **72**, 125203 (2005).

[37] C. A. Ullrich and I. V. Tokatly, Nonadiabatic electron dynamics in time-dependent density-functional theory, Phys. Rev. B **73**, 235102 (2006).

[38] M. Hellgren and U. von Barth, Exact-exchange kernel of time-dependent density functional theory: Frequency dependence and photoabsorption spectra of atoms, J. Chem. Phys. **131**, 044110 (2009).

[39] M. Thiele and S. Kümmel, Frequency Dependence of the Exact Exchange-Correlation Kernel of Time-Dependent Density-Functional Theory, Phys. Rev. Lett. **112**, 083001 (2014).

[40] M. T. Entwistle and R. W. Godby, Exact exchange-correlation kernels for optical spectra of model systems, Phys. Rev. B **99**, 161102(R) (2019).

[41] N. D. Woods, M. T. Entwistle, and R. W. Godby, Insights from exact exchange-correlation kernels, Phys. Rev. B **103**, 125155 (2021).

[42] As usual, the irreducible response function describes the response to the total field, that is, it excludes the direct Coulomb/RPA contribution.

[43] D. Mearns and W. Kohn, Frequency-dependent v-representability in density-functional theory, Phys. Rev. A **35**, 4796 (1987).

[44] It is worth noting that the first observation of zero eigenvalues for the interacting response function has been reported only in the last year [41].

[45] R. van Leeuwen, Key concepts in time-dependent density-functional theory, Int. J. Mod. Phys. B **15**, 1969 (2001).

[46] C. Verdozzi, D. Karlsson, M. P. von Friesen, C.-O. Almbladh, and U. von Barth, Some open questions in TDDFT: Clues from lattice models and Kadanoff–Baym dynamics, Chem. Phys. **391**, 37 (2011).

[47] V. Gurarie, Single-particle Green's functions and interacting topological insulators, Phys. Rev. B **83**, 085426 (2011).

[48] S. L. Adler, Quantum theory of the dielectric constant in real solids, Phys. Rev. **126**, 413 (1962).

[49] N. Wiser, Dielectric constant with local field effects included, Phys. Rev. **129**, 62 (1963).

[50] N. S. Rytova, The screened potential of a point charge in a thin film, Moscow Univ. Phys. Bull. **3**, 18 (1967).

[51] L. V. Keldysh, Coulomb interaction in thin semiconductor and semimetal films, Sov. J. Exp. Theor. Phys. Lett. **29**, 658 (1979).

[52] P. Cudazzo, I. V. Tokatly, and A. Rubio, Dielectric screening in two-dimensional insulators: Implications for excitonic and impurity states in graphane, Phys. Rev. B **84**, 085406 (2011).

[53] T. C. Berkelbach, M. S. Hybertsen, and D. R. Reichman, Theory of neutral and charged excitons in monolayer transition metal dichalcogenides, Phys. Rev. B **88**, 045318 (2013).

[54] Y. Cho and T. C. Berkelbach, Environmentally sensitive theory of electronic and optical transitions in atomically thin semiconductors, Phys. Rev. B **97**, 041409(R) (2018).

[55] D. Xiao, G.-B. Liu, W. Feng, X. Xu, and W. Yao, Coupled Spin and Valley Physics in Monolayers of MoS_2 and Other Group-VI Dichalcogenides, Phys. Rev. Lett. **108**, 196802 (2012).

[56] V. N. Kotov, V. M. Pereira, and B. Uchoa, Polarization charge distribution in gapped graphene: Perturbation theory and exact diagonalization analysis, Phys. Rev. B **78**, 075433 (2008).

[57] T. Olsen, S. Latini, F. Rasmussen, and K. S. Thygesen, Simple Screened Hydrogen Model of Excitons in Two-Dimensional Materials, Phys. Rev. Lett. **116**, 056401 (2016).

[58] M. R. Molas, A. O. Slobodeniuk, K. Nogajewski, M. Bartos, L. Bala, A. Babiński, K. Watanabe, T. Taniguchi, C. Faugeras, and M. Potemski, Energy Spectrum of Two-Dimensional Excitons in a Nonuniform Dielectric Medium, Phys. Rev. Lett. **123**, 136801 (2019).

[59] H. T. Nguyen-Truong, Exciton binding energy and screening length in two-dimensional semiconductors, Phys. Rev. B **105**, L201407 (2022).

[60] The empirical replacement $\mu \rightarrow 5\mu/4$ is aimed to fix the issue of the Nguyen-Truong [59] systematically underestimating exciton binding energies. Note that the numerical data and theoretical data compared in Fig. 2 of Ref. [59] were obtained for different values of the reduced mass which differ by a

factor 5/4 ($\mu = 0.20$ in Stier *et al.* [90] and $\mu = 0.25$ used by Nguyen-Truong). Therefore, Fig. 2 of Ref. [59] should be interpreted as the comparison of the numerical data of Stier *et al.* with the modified version of the Nguyen-Truong formula given by our Eq. (13). Indeed, our numerical calculations using the BSE confirm that our modified formula Eq. (13) produces better values of exciton binding energies in closer agreement with the numerical results than the original Nguyen-Truong formula.

[61] The numerical analysis using the BSE can improve this result for ν, suggesting a better value of $\nu \approx 0.62$, however, this difference turns out to have a minor impact on the final results of our calculation.

[62] Our code for solving Bethe-Salpeter equation for 2D massive Dirac model is publicly available at https://github.com/drgulevich/mdbse.

[63] I. Garate and M. Franz, Excitons and optical absorption on the surface of a strong topological insulator with a magnetic energy gap, Phys. Rev. B **84**, 045403 (2011).

[64] F. Wu, F. Qu, and A. H. MacDonald, Exciton band structure of monolayer MoS$_2$, Phys. Rev. B **91**, 075310 (2015).

[65] W. Zhao, Z. Ghorannevis, L. Chu, M. Toh, C. Kloc, P.-H. Tan, and G. Eda, Evolution of electronic structure in atomically thin sheets of WS$_2$ and WSe$_2$, ACS Nano **7**, 791 (2013).

[66] S. Funke, B. Miller, E. Parzinger, P. Thiesen, A. W. Holleitner, and U. Wurstbauer, Imaging spectroscopic ellipsometry of MoS$_2$, J. Phys.: Condens. Matter **28**, 385301 (2016).

[67] M. S. Diware, K. Park, J. Mun, H. G. Park, W. Chegal, Y. J. Cho, H. M. Cho, J. Park, H. Kim, S.-W. Kang, and Y. D. Kim, Characterization of wafer-scale and MoS$_2$ and WS$_2$ 2D films by spectroscopic ellipsometry, Curr. Appl. Phys. **17**, 1329 (2017).

[68] G. A. Ermolaev, D. I. Yakubovsky, Y. V. Stebunov, A. V. Arsenin, and V. S. Volkov, Spectral ellipsometry of monolayer transition metal dichalcogenides: Analysis of excitonic peaks in dispersion, J. Vac. Sci. Technol. B **38**, 014002 (2019).

[69] G. A. Ermolaev, Y. V. Stebunov, A. A. Vyshnevyy, D. E. Tatarkin, D. I. Yakubovsky, S. M. Novikov, D. G. Baranov, T. Shegai, A. Y. Nikitin, A. V. Arsenin *et al.*, Broadband optical properties of monolayer and bulk MoS$_2$, npj 2D Mater. Appl. **4**, 21 (2020).

[70] A. Gulans, S. Kontur, C. Meisenbichler, D. Nabok, P. Pavone, S. Rigamonti, S. Sagmeister, U. Werner, and C. Draxl, Exciting: a full-potential all-electron package implementing density-functional theory and many-body perturbation theory, J. Phys.: Condens. Matter **26**, 363202 (2014).

[71] H. M. Hill, A. F. Rigosi, K. T. Rim, G. W. Flynn, and T. F. Heinz, Band alignment in MoS$_2$/WS$_2$, Nano Lett. **16**, 4831 (2016).

[72] M. Rohlfing and S. G. Louie, Electron-Hole Excitations in Semiconductors and Insulators, Phys. Rev. Lett. **81**, 2312 (1998).

[73] F. Sottile, K. Karlsson, L. Reining, and F. Aryasetiawan, Macroscopic and microscopic components of exchange-correlation interactions, Phys. Rev. B **68**, 205112 (2003).

[74] F. Sottile, M. Marsili, V. Olevano, and L. Reining, Efficient ab initio calculations of bound and continuum excitons in the absorption spectra of semiconductors and insulators, Phys. Rev. B **76**, 161103(R) (2007).

[75] S. Galamić-Mulaomerović and C. H. Patterson, Ab initio many-body calculation of excitons in solid Ne and Ar, Phys. Rev. B **72**, 035127 (2005).

[76] C. A. Ullrich and Z.-h. Yang, Excitons in time-dependent density-functional theory, Top. Curr. Chem. **368**, 25805143 (2016).

[77] M. Piacentini, A new interpretation of the fundamental exciton region in LiF, Solid State Commun. **17**, 697 (1975).

[78] E. L. Shirley, L. J. Terminello, J. E. Klepeis, and F. J. Himpsel, Detailed theoretical photoelectron angular distributions for LiF(100), Phys. Rev. B **53**, 10296 (1996).

[79] We have modified values of the parameters used in Ref. [36] to align the central exciton peak frequency with that of the BSE result. In Fig. 4(a), we used $\alpha(\infty) = -8.4$ for the static and $\alpha(\omega) = -1.5 - 0.042(\omega/\text{eV})^2$ for the parabolic LRC kernel.

[80] V. Saile, M. Skibowski, W. Steinmann, P. Gürtler, E. E. Koch, and A. Kozevnikov, Observation of Surface Excitons in Rare-Gas Solids, Phys. Rev. Lett. **37**, 305 (1976).

[81] V. Saile, One- and two-photon spectroscopy with rare gas solids, Appl. Opt. **19**, 4115 (1980).

[82] S. Bernstorff and V. Saile, Experimental determination of band gaps in rare gas solids, Opt. Commun. **58**, 181 (1986).

[83] O. V. Gritsenko and E. Jan Baerends, Double excitation effect in non-adiabatic time-dependent density functional theory with an analytic construction of the exchange–correlation kernel in the common energy denominator approximation, Phys. Chem. Chem. Phys. **11**, 4640 (2009).

[84] D. M. Roessler and W. C. Walker, Optical constants of magnesium oxide and lithium fluoride in the far ultraviolet, J. Opt. Soc. Am. **57**, 835 (1967).

[85] V. Saile, Optishe Anregungen der Valenzelectronen von Argon, Krypton und Xenon in festem und gasförmigem Zustand zwischen 6 eV und 20 eV, Ph.D. thesis, Universität München, 1976.

[86] J. Sun, C.-W. Lee, A. Kononov, A. Schleife, and C. A. Ullrich, Real-Time Exciton Dynamics with Time-Dependent Density-Functional Theory, Phys. Rev. Lett. **127**, 077401 (2021).

[87] D. R. Gulevich, Y. V. Zhumagulov, A. Vagov, and V. Perebeinos, Nonadiabatic electron dynamics in time-dependent density functional theory at the cost of adiabatic local density approximation, Phys. Rev. B **100**, 241109(R) (2019).

[88] X. Jiang, Q. Zheng, Z. Lan, W. A. Saidi, X. Ren, and J. Zhao, Real-time *GW*-BSE investigations on spin-valley exciton dynamics in monolayer transition metal dichalcogenide, Sci. Adv. **7**, eabf3759 (2021).

[89] Y. V. Zhumagulov, V. D. Neverov, A. E. Lukyanov, D. R. Gulevich, A. V. Krasavin, A. Vagov, and V. Perebeinos, Nonlinear spectroscopy of excitonic states in transition metal dichalcogenides, Phys. Rev. B **105**, 115436 (2022).

[90] A. V. Stier, N. P. Wilson, K. A. Velizhanin, J. Kono, X. Xu, and S. A. Crooker, Magnetooptics of Exciton Rydberg States in a Monolayer Semiconductor, Phys. Rev. Lett. **120**, 057405 (2018).